PHYSICAL REVIEW B VOLUME 26, NUMBER 10 15 NOVEMBER 1982

Optical response of uniaxial semiconductors. II. Optical and electron-energy-loss spectra of ZrS_2 and $ZrSe_2$

H. M. Isomäki and J. von Boehm
Electron Physics Laboratory and Department of General Sciences, Helsinki University of Technology, SF-02150 Espoo 15, Finland
(Received 1 March 1982)

The permittivity, reflectivity, absorption coefficient, and electron-energy-loss spectra are calculated for ZrS_2 and $ZrSe_2$ by starting from the self-consistent Hartree-Fock-Slater results and by treating the momentum matrix elements rigorously in the bulk of the first Brillouin zone. Close agreement is found with the experimental spectra available. The peaks of the spectra are related to the band-structure features. Anisotropy and the effects of anion change are discussed. It is found that the corrections needed for an even closer agreement with the measured spectra should be opposite to and smaller than the calculated local-field—continuum-exciton corrections for Si, TlCl, and C.

I. INTRODUCTION

There exist a large number of experimental optical spectra for $1T$ layered transition-metal dichalcogenides (see the reviews by Wilson and Yoffe[1] and Evans[2]). Usually only the $\vec{E}\perp c$ component of the spectra was measured. However, the $\vec{E}\parallel c$ component would give interesting information about the anisotropy. The very recent reflectivity measurement in the range of 0.5—5 eV by Bayliss and Liang[3] shows that the $\vec{E}\perp c$ component is roughly as much as twice as large as the $\vec{E}\parallel c$ component.

On the theoretical side there exist a considerable number of calculated energy bands (see the review by Calais[4]). However, there are only very few calculations for the optical spectra of the $1T$ transition-metal dichalcogenides that start from the energy-band results. Therefore it has mostly been necessary to resort to unreliable critical-point analyses and rough joint-density-of-states analyses. However, the permittivity and thus also the reflectivity, absorption coefficient, and electron-energy-loss function depend on the energy bands via the joint density of states weighted with the momentum matrix elements. Recent calculations indicate that both the accurate joint density of states and the momentum matrix elements in the bulk of the first Brillouin zone are needed for a reliable comparison.[5] The aim of this paper is to present the results (permittivity, reflectivity, absorption coefficient, and electron-energy-loss function) of a calculation of this type for the prototype materials ZrS_2 and $ZrSe_2$.

Our calculation starts from the self-consistent Hartree-Fock-Slater results.[6,7] This allows us to study theoretically the appearance of the band-structure features as well as the anisotropy in the spectra. By comparing the spectra of ZrS_2 with those of $ZrSe_2$ we can also study the systematics with respect to the anion change. We believe that the results to be presented may serve as a useful starting point for the theoretical analysis of the response spectra of the other transition-metal dichalcogenides as well.

There has recently been a growing interest in the local-field and continuum-exciton effects in semiconductors (see the reviews by Hanke,[8] Sham,[9] and Baldereschi[10]). Quite controversial estimates have been obtained for these effects.[5,11—25] By performing detailed comparisons of the calculated spectra (not containing the local-field and continuum-exciton effects) with the experimental spectra for ZrS_2 and $ZrSe_2$ we can indirectly gain some insight into these effects. The theory and the calculational methods used for the spectra of ZrS_2 and $ZrSe_2$ were presented in the preceding paper,[26] denoted by I hereafter.

II. RESULTS AND COMPARISON WITH EXPERIMENT

The calculated densities of states (DOS) and the x-ray photoemission (XPS) results[27,28] for ZrS_2 and $ZrSe_2$ are shown in Figs. 1 and 2, respectively. Both DOS (solid lines) consist of two valence-band groups: the lower chalcogen s and the upper chalcogen p group. The three peaks of the p part of

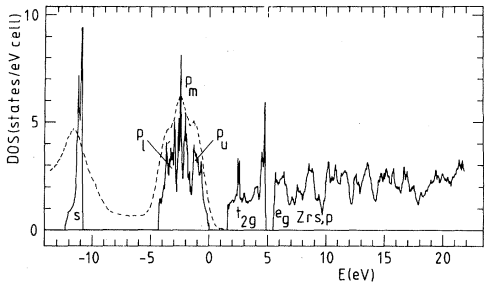

FIG. 1. Density of states of ZrS_2 (solid line). Valence-band maximum placed at the origin of the energy axis. X-ray photoemission result by Wertheim *et al.* (Ref. 27) (broken line) given in arbitrary units. Middle p_m peak of the chalcogen p group of the density of states and x-ray photoemission result set at the same energy.

DOS, denoted by p_l (lower), p_m (middle), and p_u (upper) in Figs. 1 and 2, originate from the three adjacent pairs of the p bands.[29] We notice that the increase of the number of orthogonalized plane waves (OPW) from 150 to 240 per $\vec{k}$ has improved agreement of the p part of DOS with the XPS results[27,28] (dashed lines in Figs. 1 and 2; for comparison see Ref. 29).

The first five conduction bands are of Zr 4*d* type and form two groups: the lower t_{2g} group (originating from the d_{z^2}, d_{xy}, and $d_{x^2-y^2}$ orbitals) and the upper e_g group (originating from the d_{xz} and d_{yz} orbitals).[7] The t_{2g} group appears without the d_{z^2} splitting off[7] (Figs. 1 and 2). The t_{2g} part of DOS of ZrS_2 and $ZrSe_2$ (see Figs. 1 and 2) has a two-peak form similar to that of TaS_2 calculated by Mattheiss.[30] The mixing of the e_g part with the higher Zr 5*s*,*p* part starts at 6.4 and 5.7 eV for ZrS_2 and $ZrSe_2$, respectively[7] (Figs. 1 and 2), in agreement with the tendency found experimentally by Bell and Liang.[31]

The components of the real and imaginary parts of the permittivity [$\epsilon_{1\perp}$,$\epsilon_{1\|}$ and $\epsilon_{2\perp}$,$\epsilon_{2\|}$, Eq. (47) of paper I; hereafter abbreviated as (I.47)] are presented for ZrS_2 and $ZrSe_2$ in Figs. 3 and 4, respectively. We find five main peaks in $\epsilon_{2\perp}$ [denoted by $A-E$ in Figs. 3(a) and 4(a)] at the energies 2.8, 6.5, 9.6, 10.7, and 13.0 eV for ZrS_2 and 2.6, 6.0, 8.5, 9.9, and 12.0 eV for $ZrSe_2$. These positions agree closely with those obtained from the electron-energy-loss experiment[31]: 3.0, 5.6, 10.0, and 13.2 eV for ZrS_2 and 2.1, 4.9, 9.2, and 11.5 eV for $ZrSe_2$. In this comparison we have assumed that the calculated peaks *C* and *D* correspond to the third experimental peak. However, the electron-energy-loss experiment[31] for HfS_2 yields a five-peak $\epsilon_{2\perp}$, and the comparison between the calculated and experimental reflectivities (see below) seems to give some evidence for the separate peaks *C* and *D*.

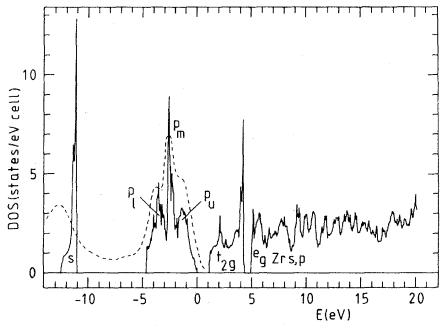

FIG. 2. Density of states of $ZrSe_2$ (solid line). X-ray photoemission result by Jellinek *et al.* (Ref. 28) (broken line) given in arbitrary units. For further information see caption of Fig. 1.

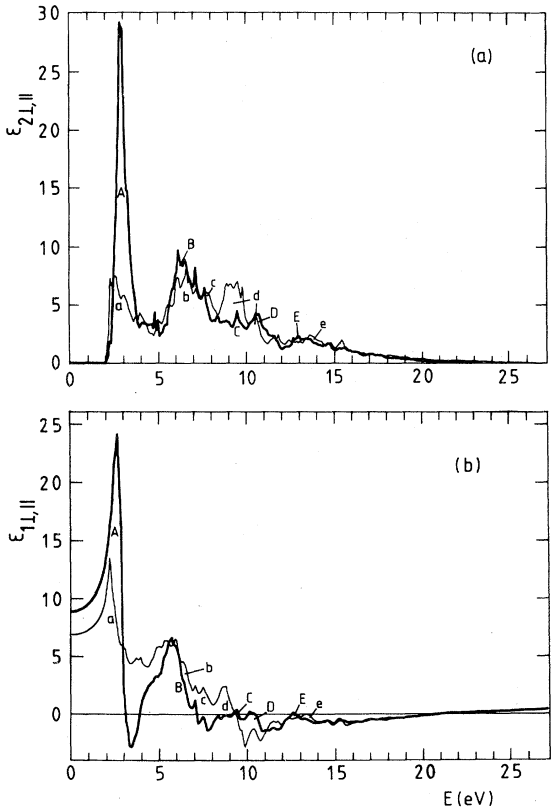

FIG. 3. Permittivity of ZrS_2. Imaginary and real parts presented in (a) and (b), respectively. Thick and thin lines represent $\vec{E}\perp c$ and $\vec{E}\|c$ components, respectively.

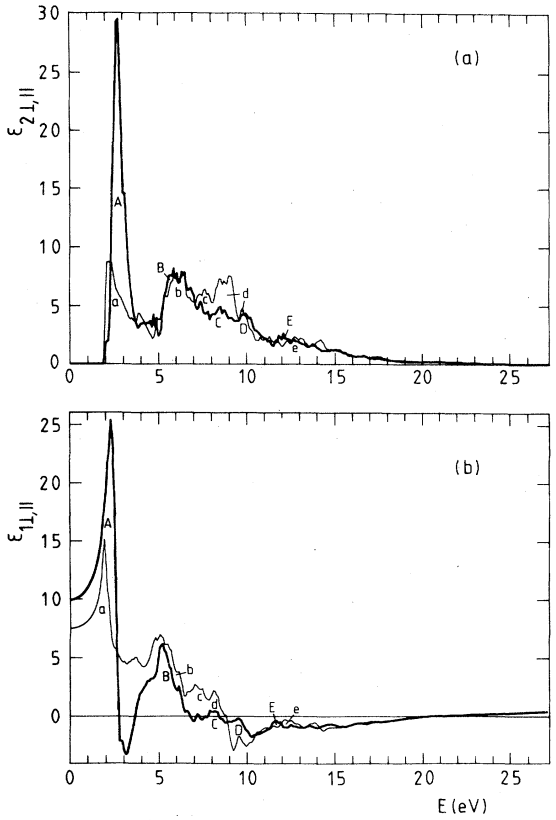

FIG. 4. Permittivity of $ZrSe_2$. For further information see caption of Fig. 3.

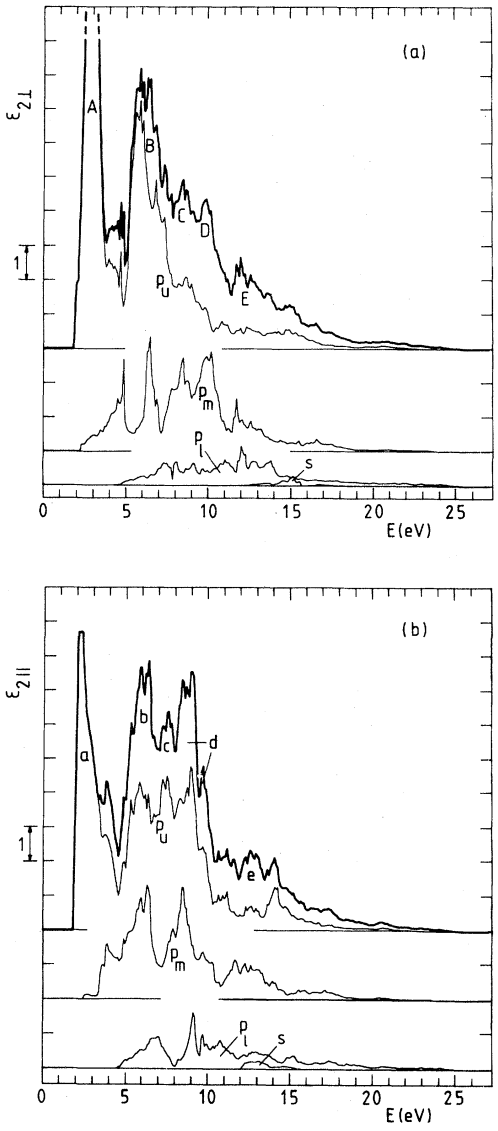

FIG. 5. Decomposition of the imaginary part of the permittivity of $ZrSe_2$. $\vec{E}\perp c$ and $\vec{E}\|c$ components presented in (a) and (b), respectively.

The decomposition of $\epsilon_{2\perp}$ and $\epsilon_{2\|}$ of $ZrSe_2$ with respect to the four (initial) valence-band pairs (s, p_l, p_m, and p_u, see Fig. 2) is shown in Fig. 5 for the analysis of the origin of peaks $A-E$ of $\epsilon_{2\perp}$ and $a-e$ of $\epsilon_{2\|}$. By comparing $\epsilon_{2\perp}$ of ZrS_2 [Fig. 3(a)] with that calculated by taking only the t_{2g} conduction bands into account,[32] we can conclude that peaks A and a are due to transitions $p_u \rightarrow t_{2g}$. In fact a closer analysis, also taking into account the decomposition with respect to the conduction bands, reveals that peaks A and a are almost entirely due to the transitions from p_u to the lowest t_{2g} band. The origin of the other peaks is obtained in the same way from Fig. 5 and by taking into account the decomposition with respect to the conduction bands. The results are summarized in Table I and are the same for both $ZrSe_2$ and ZrS_2. The contribution from the sharp p_m part resembles the conduction part of DOS (cf. Figs. 5 and 2). However, it is obvious that an analysis of the origin of the peaks by using only DOS (Fig. 2) could be quite misleading (see also Ref. 5). We also notice that the contribution from the s part to $\epsilon_{2\perp}$ and $\epsilon_{2\|}$ is almost negligible (Fig. 5).

The peaks of $\epsilon_{2\perp}$ and $\epsilon_{2\|}$ appear in $\epsilon_{1\perp}$ and $\epsilon_{1\|}$ as descending slopes accompanied by the preceding peaks. Therefore the labels of the peaks of $\epsilon_{2\perp}$ and $\epsilon_{2\|}$ are used for the corresponding features of $\epsilon_{1\perp}$ and $\epsilon_{1\|}$ [Figs. 3(b) and 4(b)]. The calculated refractive index $\epsilon_{1\perp}(\vec{0}0)^{1/2}$ of 2.97 for ZrS_2 agrees closely with the measured value 2.83 (Ref. 33). The calculated refractive index of 3.15 for $ZrSe_2$ agrees reasonably well with the measured value 3.35 (Ref. 33) and the value 2.6 derived from the measured reflectivity[34] though the experimental

TABLE I. Origin of the peaks of $\epsilon_{2\perp}$ and $\epsilon_{2||}$. Lesser contributions are in parentheses.

Spectrum	Peak	Origin
$\epsilon_{2\perp}$	A	$p_u \rightarrow$ lowest t_{2g} band
	B	$p_u \rightarrow e_g$, $p_m \rightarrow$ upper t_{2g} bands
	C	$p_m \rightarrow e_g$, $p_u \rightarrow$ lower Zr sp bands
	D	$p_m \rightarrow$ lower Zr sp bands
	E	p_m and $p_l \rightarrow$ upper Zr sp bands
$\epsilon_{2||}$	a	$p_u \rightarrow$ lowest t_{2g} band
	b	$p_u \rightarrow e_g$, p_m and $p_l \rightarrow$ upper t_{2g} bands ($p_u \rightarrow$ upper t_{2g} bands)
	c	$p_u \rightarrow e_g$ ($p_u \rightarrow$ lower Zr sp bands)
	d	$p_u \rightarrow$ lower Zr sp bands, p_m and $p_l \rightarrow e_g$
	e	p_m and $p_l \rightarrow$ upper Zr sp bands

values differ too much from each other to allow a reliable comparison.

The calculated reflectivity components [$R_\perp$ and $R_{||}$, Eq. (I.52)] and the experimental components[3,34–36] are shown in Figs. 6 and 7 for ZrS_2 and $ZrSe_2$, respectively (solid and dashed or dashed-dotted lines represent the calculated and experimental curves, respectively). The main peaks of $\epsilon_{2\perp}$ and $\epsilon_{2||}$ appear in $R_\perp$ and $R_{||}$ as modified peaks at slightly higher energies. Therefore the labels of the peaks of $\epsilon_{2\perp}$ and $\epsilon_{2||}$ are used for the corresponding peaks of $R_\perp$ and $R_{||}$, and the analysis of Table I applies to the peaks of $R_\perp$ and $R_{||}$ as well. The calculated $R_\perp$ and $R_{||}$ agree closely with the measured ones (Figs. 6 and 7). The main peaks A, B, and D are distinct in the measured $R_\perp$. We associate the structure between the measured peaks B and D with peak C (Figs. 6 and 7), which is most distinct in the measured $R_\perp$ of ZrS_2 by Hughes and Liang[35] (Fig. 6). The steep decrease of the calculated $R_\perp$ and $R_{||}$ of ZrS_2 ($ZrSe_2$) above $\sim$20 (19) eV as well as that of the measured $R_\perp$ of $ZrSe_2$ by Mamy *et al.*[36] above 19 eV represents the plasma edge (Figs. 6 and 7). The difference between the calculated and measured $R_\perp$ for $ZrSe_2$ above 13 eV may mainly be due to the effect of surface contamination and/or damage involved in the measured $R_\perp$ (Ref. 36) (Fig. 7). In fact, the $R_\perp$ measured by Hughes and Liang[35] for samples having high-quality surfaces increases steeply above $\sim$12 eV, in agreement with the cal-

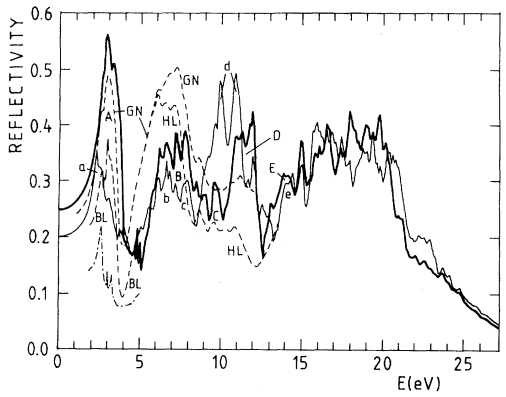

FIG. 6. Reflectivity of ZrS_2. Thick and thin solid lines represent $\vec{E}\perp c$ and $\vec{E}||c$ components of the calculated reflectivity, respectively. Dashed lines represent experimental $\vec{E}\perp c$ components by Greenaway and Nitsche (Ref. 34), Hughes and Liang (Ref. 35), and Bayliss and Liang (Ref. 3) denoted by GN, HL, and BL, respectively. Dashed-dotted line represents the experimental $\vec{E}||c$ component by Bayliss and Liang (Ref. 3).

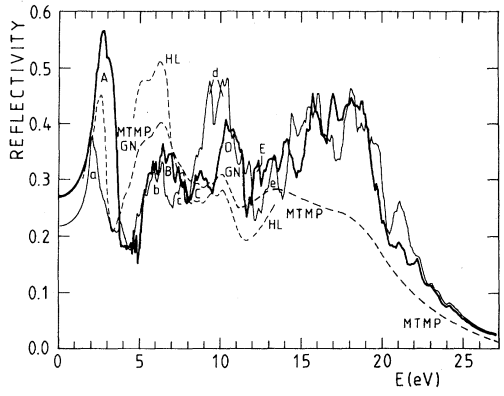

FIG. 7. Reflectivity of $ZrSe_2$. Thick and thin solid lines represent $\vec{E}\perp c$ and $\vec{E}||c$ components of the calculated reflectivity, respectively. Dashed lines represent the experimental $\vec{E}\perp c$ components by Greenaway and Nitsche (Ref. 34), Hughes and Liang (Ref. 35), and Mamy *et al.* (Ref. 36) denoted by GN, HL, and MTMP, respectively. GN and MTMP reflectivity are practically identical up to $\sim$11 eV and are represented by a single curve.

culated $R_\perp$ (Figs. 6 and 7). (A more thorough discussion about the effects of surface contamination and/or damage is given in the next paper.[37])

The calculated absorption coefficient [$K_\perp$ and $K_{||}$ Eq. (I.53)] as well as the measured $K_\perp$ by Beal *et al.*[38] for ZrS_2 and $ZrSe_2$ are shown in Figs. 8 and 9, respectively (the solid and dashed lines represent the calculated and measured absorption coefficients, respectively). The peaks of $\epsilon_{2\perp}$ and $\epsilon_{2||}$ appear in $K_\perp$ and $K_{||}$ as modified peaks. Therefore the labels of the peaks of $\epsilon_{2\perp}$ and $\epsilon_{2||}$ are used for the corresponding peaks of $K_\perp$ and $K_{||}$, and the analysis of Table I applies to the peaks of $K_\perp$ and $K_\perp$ and $K_{||}$ as well. The calculated $K_\perp$ agree with the measured $K_\perp$ (Ref. 38) (including essentially only peak *A*) quite closely (Figs. 8 and 9). Because the sum rule is accurately valid for the calculated $K_\perp$ (see paper I) the difference from the measured $K_\perp$ may, at least partly, be due to inaccuracies in the scaling of the experimental $K_\perp$ (Ref. 38).

The calculated components of the electron-energy-loss function, $-\mathrm{Im}\epsilon_\perp^{-1}$ and $-\mathrm{Im}\epsilon_{||}^{-1}$ (see paper I), as well as the measured $-\mathrm{Im}\epsilon_\perp^{-1}$ by Bell and Liang,[31] are shown in Figs. 10 and 11 for ZrS_2 and $ZrSe_2$, respectively. The origin and position of the main loss peaks are summarized in Table II. The loss peaks are basically due to the valleys between the main peaks of $\epsilon_{2\perp}$ and $\epsilon_{2||}$ (Table II) except the last (largest) peak (L_5,l_5) which is the plasma peak (associated with the change of $\epsilon_{1\perp}$ or $\epsilon_{1||}$ from negative to positive for the last time). The positions of the peaks L_1-L_5 of the calculated and measured $-\mathrm{Im}\epsilon_\perp^{-1}$ agree remarkably closely (Table II) (the closely lying peaks L_2 and L_3 correspond to one peak in the experimental

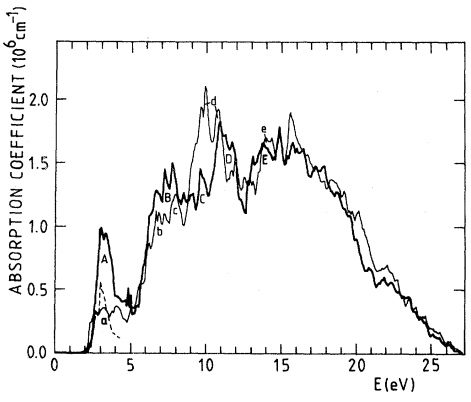

FIG. 8. Absorption coefficient of ZrS_2. Thick and thin solid lines represent the calculated $\vec{E}\perp c$ and $\vec{E}||c$ components, respectively. Broken line represents the measured $\vec{E}\perp c$ component by Beal *et al.* (Ref. 38).

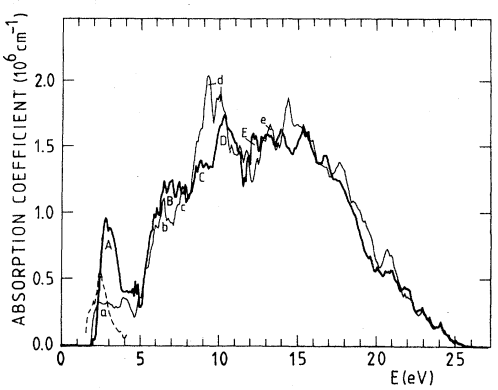

FIG. 9. Absorption coefficient of $ZrSe_2$. For further information see caption of Fig. 8.

$-\mathrm{Im}\epsilon_\perp^{-1}$). The free-electron plasma frequencies of 18.1 and 17.1 eV for ZrS_2 and $ZrSe_2$, respectively, are $\sim 2-4$ eV lower than the calculated and measured values (Table II). This is in accordance with the theory by Pines,[39] which states that if the major part of the optical transitions falls below the free-electron plasma frequency [Figs. 3(a) and 4(a)] the effect of the transitions is to shift the plasma frequency (anisotropically) towards a higher energy and also to broaden the resulting plasma peaks (Figs. 10 and 11).

III. ANISOTROPY, EFFECTS OF ANION CHANGE, AND LOCAL-FIELD AND CONTINUUM-EXCITON EFFECTS

The origin for the main anisotropy of the spectra (difference between the perpendicular and parallel components) obtained by using Table I and

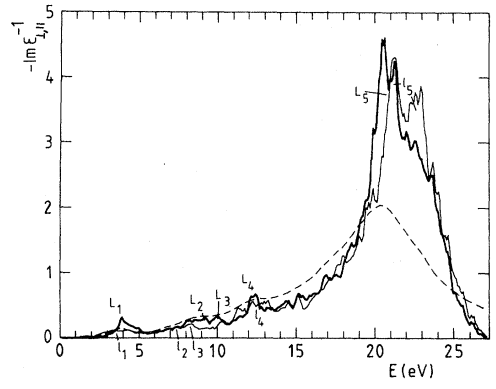

FIG. 10. Electron-energy-loss function of ZrS_2. Thick and thin solid lines represent the calculated $-\mathrm{Im}\epsilon_\perp^{-1}$ and $-\mathrm{Im}\epsilon_{||}^{-1}$, respectively. Broken line represents measured $-\mathrm{Im}\epsilon_\perp^{-1}$ by Bell and Liang (Ref. 31).

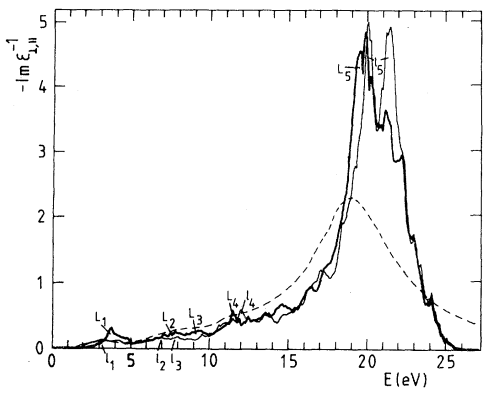

FIG. 11. Electron-energy-loss function of $ZrSe_2$. For further information see caption of Fig. 10.

the decomposition of Fig. 5 is given in Table III. Table III shows that the transitions from the uppermost valence-band pair p_u are mainly responsible for the anisotropy in the spectra up to about 10 eV. The transitions from the second uppermost valence-band pair p_m are most important for the anisotropy above 10 eV. Our calculation reproduces the anisotropy of the measured reflectivity by Bayliss and Liang[3] at 0.5—5 eV remarkably well (Fig. 6).

The difference between the peaks A of $\epsilon_{2\perp}$ and a of $\epsilon_{2\parallel}$ [Figs. 3(a) and 4(a)] is reflected in the difference between the peaks L_1 of $-\mathrm{Im}\epsilon_{\perp}^{-1}$ and l_1 of $-\mathrm{Im}\epsilon_{\parallel}^{-1}$ (Figs. 10 and 11). The distinct difference between the plasma peaks L_5 and l_5 (Figs. 10 and 11, Table II) seems to be due to the transitions from the lowest valence-band pair p_l (see Fig. 5).

As to the effects of the anion change, the calculated spectra of ZrS_2 and $ZrSe_2$ are very similar (cf. Figs. 3, 4, and 6—11), but the spectra of (more metallic) $ZrSe_2$ are slightly compressed along the energy axis compared with those of ZrS_2. The main peaks of the calculated permittivity, absorption coefficient, and loss function of $ZrSe_2$ are generally slightly higher than those of ZrS_2, in accordance with the requirements of the sum rules (see paper I and cf. Figs. 3, 4, and 8—11).

The local-field and the local-field—continuum-exciton corrections are neglected in the present study. The latter corrections for Si (Refs. 13 and 14) and TlCl (Refs. 17 and 18) increased $\epsilon_1(\vec{0}0)$ and the first peak of ϵ_2 relative to the second one by a factor of ~ 2, improving agreement with the experimental spectra. Above, we found for the calculated $R_\perp$ of ZrS_2 and $ZrSe_2$ that the first peak A (and a of $R_\parallel$ of ZrS_2) was higher and the second peak B was lower than the corresponding experimental one. Compatibly with this and in agreement with Refs. 23, 24, and 37, the calculated $\epsilon_{1\perp}(\vec{0}0)$ of ZrS_2 (and, with reservations, that of $ZrSe_2$) was slightly larger than the experimental one. Thus, the corrections needed for ZrS_2 and $ZrSe_2$ should be *opposite* to and *smaller* than the calculated local-field—continuum-exciton corrections for Si (Refs. 13 and 14) and TlCl (Refs. 17 and 18) [and also for C (Ref. 25)]. (Small local-field corrections, like those found by Van Camp *et al.* for Si,[15] would bring the calculated spectra for ZrS_2 and $ZrSe_2$ to closer agreement with the measured ones.) The above discrepancy is not due to the fact that we use Slater's exchange-correlation potential,[40] since the uncorrelated, and the correlated, as well as the correlated and self-energy—corrected, Dirac-Gáspár-Kohn-Sham po-

TABLE II. Origin and position of the peaks of the electron-energy-loss function. Numbers are given in eV. A peak in $-\mathrm{Im}\epsilon_{\perp}^{-1}$ or $-\mathrm{Im}\epsilon_{\parallel}^{-1}$ corresponds to a valley in $\epsilon_{2\perp}$ or $\epsilon_{2\parallel}$. For example, *A-B* in the third column denotes the valley between the peaks A and B of $\epsilon_{2\perp}$.

			ZrS_2		$ZrSe_2$	
Spectrum	Peak	Origin	Theor.[a]	Expt.[b]	Theor.[a]	Expt.[b]
$-\mathrm{Im}\epsilon_{\perp}^{-1}$	L_1	*A-B*	4.0	4	3.8	3
	L_2	*B-C*	9.3	9	7.9	7.5
	L_3	*C-D*	10.1		9.4	
	L_4	*D-E*	12.3	12.1	11.5	11.5
	L_5	plasma	20.9	20.3	19.6	19.1
$-\mathrm{Im}\epsilon_{\parallel}^{-1}$	l_1	*a-b*	3.9		3.5	
	l_2	*b-c*	7.3		6.8	
	l_3	*c-d*	8.4		8.0	
	l_4	*d-e*	12.5		12.0	
	l_5	plasma	22.0		20.6	

[a]Present study.

[b]Bell and Liang (Ref. 31).

TABLE III. Origin of the main anisotropy regions of the calculated optical spectra.

Spectrum	Region (eV) ZrS_2	Region (eV) $ZrSe_2$	Origin
$\epsilon_{2\perp},\epsilon_{2\parallel}$	2–4	2–3.5	$p_u\rightarrow$ lowest t_{2g} band
	6–7	7–8	$p_u\rightarrow e_g$ ($p_m\rightarrow t_{2g}$)
	8.5–10	8–9.5	$p_u\rightarrow$ Zr sp
	10.5–11.5	10–11	$p_m\rightarrow$ Zr sp
$\epsilon_{1\perp},\epsilon_{1\parallel}$	0–4	0–4	$p_u\rightarrow$ lowest t_{2g} band
	7–11	6.5–10.5	$p_u\rightarrow e_g$, $p_u\rightarrow$ Zr sp, $p_m\rightarrow$ Zr sp
$R_\perp,R_\parallel$	0–4	0–3.5	$p_u\rightarrow$ lowest t_{2g} band
	6–8.5	6–7.5	$p_u\rightarrow e_g$ ($p_m\rightarrow t_{2g}$)
	9–10.5	8–9.5	$p_u\rightarrow$ Zr sp
	10.5–12	9.5–11	$p_m\rightarrow$ Zr sp
$K_\perp,K_\parallel$	2.5–4	2–4	$p_u\rightarrow$ lowest t_{2g} band
	6–8	6–7.5	$p_u\rightarrow e_g$ ($p_m\rightarrow t_{2g}$)
	8.5–10	8–9.5	$p_u\rightarrow$ Zr sp
	10–12	9.5–11.5	$p_m\rightarrow$ Zr sp

tential[41–47] would underestimate the smallest transitions more than Slater's potential, thereby making the first peak A (a) of $R_\perp$ and $\epsilon_{2\perp}$ ($R_\parallel$ and $\epsilon_{2\parallel}$) for ZrS_2 and $ZrSe_2$ even higher.

The very different results for the permittivities with and without the local-field and continuum-exciton corrections show that there is still much to be learned before even a qualitative picture about these corrections may be obtained. We feel that the main problem with the local theories is the fact that they underestimate the smallest transitions (including the minimum optical gap) and that there is no systematic way to improve the results (in contrast to the Hartree-Fock theory). Nevertheless, according to our results it seems that one could advance much further also within the local theories (without the local-field and continuum-exciton corrections) provided that the band structure and the momentum matrix elements are calculated rigorously up to sufficiently high energies.

IV. CONCLUSIONS

We have presented for ZrS_2 and $ZrSe_2$ the theoretical permittivity, reflectivity, absorption coefficient, and electron-energy-loss spectra based on the self-consistent band-structure results and the rigorous calculation of the momentum matrix elements. Close agreement was obtained with the experimental spectra. It was found that the first peak (A or a) of the permittivity, reflectivity, and absorption coefficient is due to the transitions from the uppermost valence-band pair p_u. The next peaks B, C, and D or b, c, and d, forming the second broad maximum, are due both to the transitions from p_u and to those from the second uppermost valence-band pair p_m. The main anisotropies $A\leftrightarrow a$ and $D\leftrightarrow d$ are mainly due to the anisotropy in the transitions from p_u. The comparison of the calculated spectra of ZrS_2 and $ZrSe_2$ with the measured spectra shows that the corrections needed for closer agreement should be *opposite* to and *smaller* than the calculated local-field–continuum-exciton corrections for Si,[13,14] TlCl,[17,18] and C.[25]

ACKNOWLEDGMENTS

We would like to thank Professor T. Stubb and Professor M. A. Ranta for their support and Dr. S. C. Bayliss and Dr. W. Y. Liang for sending their results and giving permission to refer to their work prior to its publication.

[1]J. A. Wilson and A. D. Yoffe, Adv. Phys. 18, 193 (1969).

[2]B. L. Evans, in *Optical and Electrical Properties,* edited by P. A. Lee (Reidel, Dordrecht, 1976), p. 1.

[3]S. C. Bayliss and W. Y. Liang, J. Phys. C 15, 1283 (1982).

[4]J.-L. Calais, Adv. Phys. 26, 847 (1977).

[5]H. M. Isomäki and J. von Boehm, J. Phys. C 14, L1043

(1981).
[6]H. Isomäki and J. von Boehm, Phys. Scr. 24, 465 (1981).
[7]H. M. Isomäki and J. von Boehm, Phys. Lett. A 89, 89 (1982).
[8]W. Hanke, Adv. Phys. 27, 287 (1978).
[9]L. J. Sham, J. Phys. Soc. Jpn. 49, Suppl. A, 69 (1980).
[10]A. Baldereschi, J. Phys. Soc. Jpn. 49, Suppl. A, 155 (1980).
[11]J. A. Van Vechten and R. M. Martin, Phys. Rev. Lett. 28, 446 (1972).
[12]S. G. Louie, J. R. Chelikowsky, and M. L. Cohen, Phys. Rev. Lett. 34, 155 (1975).
[13]W. Hanke and L. J. Sham, Phys. Rev. Lett. 43, 387 (1979).
[14]W. Hanke and L. J. Sham, Phys. Rev. B 21, 4656 (1980).
[15]P. E. Van Camp, V. E. Van Doren, and J. T. Devreese, Phys. Rev. B 24, 1096 (1981).
[16]R. Riedinger and M. A. Khan, Philos. Mag. B 44, 547 (1981).
[17]W. Schäfer, M. Schreiber, and J. Treusch, J. Phys. Soc. Jpn. 49, Suppl. A, 81 (1980).
[18]W. Schäfer and M. Schreiber, Solid State Commun. 38, 1241 (1981).
[19]M. Kastner and R. R. Forberg, Phys. Rev. Lett. 36, 740 (1976).
[20]H. Wendel, R. M. Martin, and D. J. Chadi, Phys. Rev. Lett. 38, 656 (1977).
[21]J. D. Joannopoulos, Th. Starkloff, and M. Kastner, Phys. Rev. Lett. 38, 660 (1977).
[22]F. Nizzoli, in *The Physics of Selenium and Tellurium,* edited by E. Gerlach and P. Grosse (Springer, Berlin, 1979), p. 31.
[23]C. S. Wang and B. M. Klein, Phys. Rev. B 24, 3417 (1981).
[24]H. M. Isomäki, Phys. Rev. B 26, 4485 (1982).
[25]W. Hanke and L. J. Sham, Phys. Rev. B 12, 4501 (1975).
[26]J. von Boehm and H. M. Isomäki, preceding paper, Phys. Rev. B 26, 5798 (1982) (paper I).
[27]G. K. Wertheim, F. J. DiSalvo, and D. N. E. Buchanan, Solid State Commun. 13, 1225 (1973).
[28]F. Jellinek, R. A. Pollak, and M. W. Shafer, Mater. Res. Bull. 9, 845 (1974).
[29]J. von Boehm and H. Isomäki, J. Phys. C 13, 3181 (1980).
[30]L. F. Mattheiss, Phys. Rev. B 8, 3719 (1973).
[31]M. G. Bell and W. Y. Liang, Adv. Phys. 25, 53 (1976).
[32]H. Isomäki and J. von Boehm, Physica B105, 156 (1981). In this paper "cell" in Fig. 1(a) should be replaced by a_0^3 (a_0 is the Bohr radius).
[33]P. A. Lee, G. Said, R. Davis, and T. H. Lim, J. Phys. Chem. Solids 30, 2719 (1969).
[34]D. L. Greenaway and R. Nitsche, J. Phys. Chem. Solids 26, 1445 (1965).
[35]H. P. Hughes and W. Y. Liang, J. Phys. C 10, 1079 (1977).
[36]R. Mamy, B. Thieblemont, L. Martin, and F. Pradal, Nuovo Cimento B 38, 196 (1977).
[37]H. M. Isomäki, J. von Boehm, and T. Stubb, following paper, Phys. Rev. B 26, 5815 (1982) (paper III).
[38]A. R. Beal, J. C. Knights, and W. Y. Liang, J. Phys. C 5, 3531 (1972).
[39]D. Pines, Rev. Mod. Phys. 28, 184 (1956).
[40]J. C. Slater, Phys. Rev. 81, 385 (1951).
[41]P. A. M. Dirac, Proc. Cambridge Philos. Soc. 26, 376 (1930).
[42]R. Gáspár, Acta Acad. Sci. Hung. 3, 263 (1954).
[43]W. Kohn and L. J. Sham, Phys. Rev. 140, A1133 (1965).
[44]E. Wigner, Phys. Rev. 46, 1002 (1934).
[45]L. Hedin and B. I. Lundqvist, J. Phys. C 4, 2064 (1971).
[46]L. J. Sham and W. Kohn, Phys. Rev. 145, 561 (1966).
[47]M. Schreiber and W. Schäfer, Phys. Rev. B 21, 3571 (1980).